ELSEVIER

Earth and Planetary Science Letters 195 (2002) 75–90

EPSL

www.elsevier.com/locate/epsl

Vanadium in peridotites, mantle redox and tectonic environments: Archean to present

Dante Canil *

School of Earth and Ocean Sciences, University of Victoria, 3800 Finnerty Rd., Victoria, BC, Canada V8W 3P6

Received 6 May 2001; received in revised form 17 October 2001; accepted 16 November 2001

Abstract

New measurements of partition of vanadium (V) between spinel, garnet and a pigeonite-like high pressure (*P*) pyroxene and magnesian liquids on the mantle solidus as a function of oxygen fugacity (fO_2) are presented. The spinel-liquid experiments show an effect of Cr/Al in spinel on partitioning, and further suggest that V exists as V^{3+}, V^{4+} and V^{5+} in melts at terrestrial fO_2. Vanadium is mildly incompatible in both 'pigeonitic' pyroxene and garnet between 4.5 and 6.5 GPa on the mantle solidus. Analysis of the fO_2-sensitive partitioning for V between mantle minerals and melts are combined with compositional data from peridotite melting experiments to model the covariation of V and Al in peridotite residues produced by non-modal, fractional melting under different fO_2 from 1.0 to 7.0 GPa. The partial melting models at 1.0 to 3.0 GPa fit the covariation of V and Al in abyssal peridotites quite well at fO_2s similar to those of mid-ocean ridge basalt. Many orogenic massifs and spinel lherzolite xenoliths represent mantle that formed at fO_2 higher than that produced at mid-ocean ridges in a range of tectonic environments. A large proportion of spinel-facies Archean cratonic lithosphere formed at fO_2s significantly higher than those of abyssal peridotites possibly linking its formation to a convergent margin (arc) tectonic setting. The case for garnet-facies cratonic mantle is equivocal; it may have formed at significantly higher pressures (7.0 GPa), or within the spinel-facies at lower pressures but at significantly higher fO_2 than is observed for abyssal peridotites. The imbrication of both oceanic garnet-facies mantle with spinel-facies arc mantle may explain the datasets for some Archean cratons. Overall, the data for Archean mantle melts and residues make clear that models cannot look to reduced, mantle-derived volcanic gases containing H_2 and CO to engender early life synthesis, or to promote hydrogen escape and gradual oxygenation of the Archean earth system.

Keywords: mantle; oxygen; fugacity; lithosphere; peridotites; vanadium; partitioning

1. Introduction

An understanding of the origin of mantle lithosphere in diverse geological settings addresses a rich variety of questions such as the origin of the continents, the rheology of the lithosphere, and its role in orogeny or as a geochemical reservoir [1,2]. The prevailing fO_2 during the formation of mantle lithosphere bears on the geochemical history and mass transfer of the atmophile elements (C, H, S, N) between the Earth's mantle, crust, and exosphere (hydro+atmosphere) [3,4]. The redox states of mantle-derived magmas

* Tel.: +1-250-472-4180; Fax: +1-250-721-6200.
E-mail address: dcanil@uvic.ca (D. Canil).

0012-821X/02/$ – see front matter
PII: S0012-821X(01)00582-9

clearly vary with tectonic setting [5,6] a trend that appears to be preserved in volcanic rocks as old as Archean [7,8] but a complementary spatial and secular variation in the fO_2 during formation of mantle lithosphere remains obscure. Although the fO_2 of mantle lithosphere can be recorded by mineral equilibria in peridotites at the time of their exhumation [9] it is not clear whether these fO_2 values represent those at the time of original lithosphere formation or of later processes, because oxygen is generally poorly buffered in the upper mantle [10].

This study attempts to unravel the paleo-redox states during formation of mantle lithosphere using the vanadium (V) abundances of peridotites. New measurements on the fO_2-sensitive partitioning of V between spinel, garnet, pyroxene, and melt along the peridotite solidus, in addition to similar measurements on olivine, orthopyroxene and high Ca clinopyroxene [7,11–13], are combined with data from peridotite melting experiments to construct fractional melting models of the abundance of V in peridotite residues produced under different P and fO_2. The residue trends from the melting models are compared to a large database for peridotites from different tectonic settings from Archean to Phanerozoic. The new melting models provide an independent test of inferences that the fO_2 of the Archean mantle was as high as that of today [8,11] and have implications for the tectonic environment for the formation of Archean mantle roots and for Precambrian atmospheric evolution.

2. Behavior of V during igneous and metamorphic processes

V exists in four potential valence states in magmas, V^{2+}, V^{3+}, V^{4+} and V^{5+}. In melts at terrestrial fO_2s only V^{3+}, V^{4+} and V^{5+} are likely to be present, the abundance of V^{4+} and V^{5+} is small, and the proportion of V^{3+} (or the $V^{3+}/\Sigma V$ ratio) decreases substantially with increasing fO_2 [7]. The crystal structures of most liquidus phases in mafic and ultramafic magmas prefer to incorporate V^{3+}, and for this reason experimentally measured $D_V^{crystal/liquid}$ (which is the sum of $D_{(V^{2+}, V^{3+}, V^{4+}, V^{5+})}$) decreases with increasing fO_2 [14]. In this way, increased fO_2 during melting or crystallization will decrease the overall compatibility of V, as it does for Fe. Unlike Fe, however, post-igneous changes in the $V^{3+}/\Sigma V$ ratio of a rock are irrelevant, it need only remain a closed system with respect to its bulk V abundance to preserve its original igneous redox memory. The low mobility of V during alteration and metamorphism favors the preservation of this redox memory even in rocks more than 3 Ga old [8].

As a mildly incompatible element, the potential exists for V to be re-distributed during the complex history of mantle samples that is often recorded by strongly incompatible elements and their isotopes (e.g. Sr, Nd, Pb). Nonetheless, post-melting phenomena in the mantle lithosphere do not appear to play a major role in re-distributing V. This is clearly evidenced in the Ronda peridotite, for which field and isotopic studies document a long and complex igneous, metamorphic and tectonic evolution [15], and yet there is no apparent disturbance of the melt depletion trend for V [16].

The mildly incompatible behavior of V during partial melting in the mantle is largely controlled by clinopyroxene and spinel until these phases are exhausted after about 25% melting [12]. Garnet and a low Ca 'pigeonitic' pyroxene appear on the mantle solidus above 2.8 GPa [17] and could also potentially control V partitioning between melt and residue, but this inference remains to be tested by experiment.

3. Experiments

3.1. Spinel–liquid

At a given fO_2 $D_V^{sp/liq}$ shows a larger variation than has so far been observed for any other phase on the mantle solidus [12]. To model more accurately and understand the behavior of V during partial melting in the spinel peridotite stability field, $D_V^{sp/liq}$ was measured in this study in three different compositions under variable fO_2 (Table 1). Two starting compositions were komatiites (*adk, auk*) specifically chosen to have olivine and

spinel in equilibrium with picritic melts at temperatures within the melting range of peridotite at pressures below 3 GPa. A third starting composition (AnFo30) in the system Fo–An was chosen to investigate $D_V^{sp/liq}$ in a far simpler system where spinel is on the liquidus [18] and to confirm the valency of V substituting into spinel as a function of fO_2.

The partitioning experiments on all three compositions were performed at 100 kPa using the Pt wire loop method with techniques described previously [7]. Polished run products mounted in epoxy were analyzed by electron microprobe (EMP) using 100 s count times for V in spinel and glass (Table 2, **Background Data Set**[1]). Some spinel analyses with inordinately high Si contents (>0.5 wt% SiO_2) were rejected due to excitation from nearby glass. Only grains 10 μm or larger could be reliably analyzed by EMP. Experiments were not reversed but equilibrium is suggested by the convergent results produced for the two different komatiite starting materials, and the lack of observable zoning in any phase.

The partitioning of trace elements (La, Yb, Zr, Yb, Zn, Ga, V) between olivine and liquid in the komatiite experiments was measured in a previous study by laser ablation inductively coupled plasma mass spectrometry (LA-ICP-MS) [13]. In this study, some of these trace elements were not determined in coexisting spinel grains because they were too small to be analyzed by LA-ICP-MS. Of the trace elements added only Ga, Zn, and Sc partition in any significant amount into spinel [19]. Using the concentration of these elements determined by LA-ICP-MS in the coexisting glass [13], and assuming the $D_{Ga,Zn,Sc}^{sp/liq}$ values of Horn [19] the spinel in these experiments likely contained on the order of 460 ppm Ga, 4 ppm Zn and 145 ppm Sc. These concentrations are not expected to affect the $D_V^{sp/liq}$ values in any way.

3.2. Garnet- and 'pigeonite'-liquid

At pressures above 2.8 GPa on the mantle solidus, garnet replaces spinel, and low- and high-Ca pyroxenes converge in composition to a 'pigeonite'-like pyroxene, replacing orthopyroxene as a subsolidus mineral [20]. To investigate the role of these phases in V partitioning at higher pressures during melting, the partitioning of V between garnet, pyroxene and ultramafic liquid along the mantle solidus was measured in run products of melting experiments between 4.5 and 6.5 GPa on natural fertile peridotite KLB1 (Table 1). All but one of these run products were previously described in detail [21] but were re-investigated analytically in this study (Table 3, **Background Data Set**[1]). Low levels of V in small grains (<30 μm) of garnet and pyroxene were determined using 300 s counting times for V by EMP. In larger grains (>80 μm) of coexisting olivine, pyroxene and in pools of ultramafic liquid, V concentrations were determined by LA-ICP-MS using a Merchantek Geolase™ LUV266 Nd-YAG UV laser system coupled to a VG™ quadrupole PQIIS ICP-MS at the University of Victoria. Laser spot diameters were 30 μm for olivine and pyroxene and 100 μm for quenched liquid. Details of the instrumentation, operating

Table 1
Starting compositions for experiments[a]

Sample	*auk*	*adk*	AnFo30	KLB1
Na_2O				0.3
MgO	19.4	20.1	42.9	39.2
Al_2O_3	9.4	5.9	25.6	3.6
SiO_2	44.5	48.7	17.1	44.5
CaO	9.9	9.8	14.1	3.44
TiO_2	0.61	0.6		0.16
Cr_2O_3	2	2		0.31
MnO				0.12
FeO	9.3	9.4		8.1
Total	98.3	98.9	99.7	99.73
V (ppm)	714	646	836	82

These compositions were synthesized from mixtures of reagent grade $CaCO_3$, MgO, SiO_2, Al_2O_3 Fe_2O_3, $ZnCO_3$, Ni and V_2O_5 and fused into glasses at 1500°C in air. Oxides of La_2O_3, Yb_2O_3, Sc_2O_3, GeO_2, Ga_2O_3 and ZrO_2 (to a total of 2.5 wt%) were then added to the mixture, followed by regrinding, a second fusion and final grinding to a powder with 2 wt% Cr_2O_3 added to promote spinel saturation. Glass of AnFo30 doped with ~840 ppm V was synthesized from oxides as described above.

[a] EMP analyses of starting glasses, except KLB1 which is a bulk rock analysis [21].

[1] http://www.elsevier.com/locate/epsl

conditions, calibration and data reduction are described elsewhere [12,22]. Precision and accuracy based on analysis of standard basalt glass BCR-2 is better than 5% for V [12]. In each sample at least three different spots of each phase were analyzed.

All the KLB1 experiments were carried out in graphite capsules using techniques described previously [21] except for run #979 (Table 3, **Background Data Set**[1]) in which the starting material was loaded in a Re capsule, surrounded by a mixture of Re and ReO_2 powder packed in a second Re capsule in an effort to buffer the charge at the Re-ReO_2 buffer. The fO_2 in these experiments cannot be externally controlled but can be measured using the fO_2-sensitive partitioning of V between olivine and liquid [11,13]. In experiment #601 (Table 3, **Background Data Set**[1]) the fO_2 determined by olivine-liquid V partitioning for V was cross-checked with that measured by the Fe content in a 30 μm diameter Pt wire loaded in the charge [23]. The two techniques produced fO_2 estimates within error of one another (Table 3, **Background Data Set**[1]), confirming the utility and accuracy of the olivine-liquid V partitioning technique for estimation of fO_2 in high pressure melting experiments.

4. Results

4.1. Spinel–liquid

At 1375°C, the two komatiite compositions saturate with olivine and spinel whereas the AnFo30 composition saturates only with spinel (Table 2, **Background Data Set**[1]). Spinels in all compositions crystallized as cubes and octahedra less than 20 μm in size. Spinels in the *auk* and *adk* compositions formed both inside and outside of olivine grains. At a given fO_2, the *adk* and *auk* komatiites have $D_V^{sp/liq}$ that are within error of one another (Fig. 1a) whereas the AnFo30 composition produces generally lower $D_V^{sp/liq}$ (Fig. 1a). All compositions show a similar S-shaped covariance of $D_V^{sp/liq}$ with fO_2 typical of the partitioning of other polyvalent elements (e.g. Cr, Fe) in magmas [24].

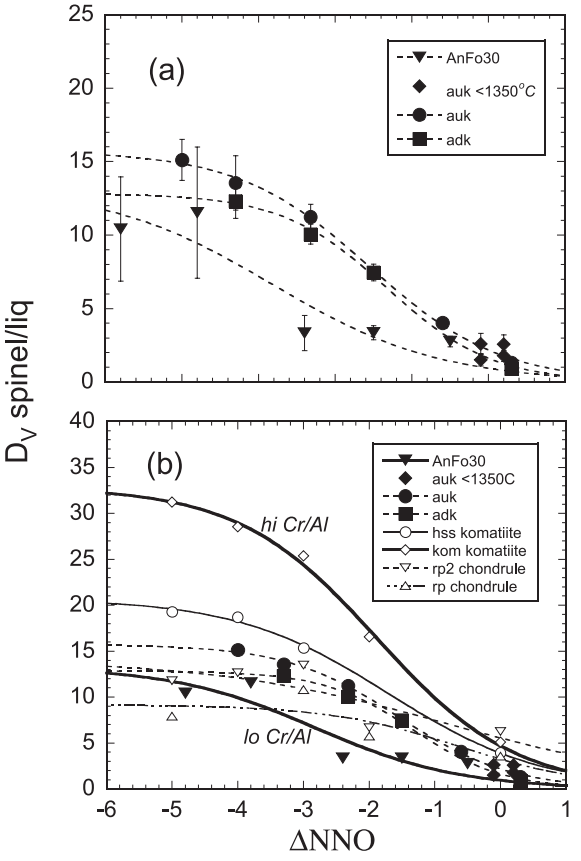

Fig. 1. Covariation of $D_V^{sp/liq}$ with fO_2 relative to the nickel–nickel oxide buffer ($\Delta NNO = fO_2$ experiment $- fO_2$ NNO buffer at P and T). T–fO_2 values for NNO buffer from [59]. Trend lines fitted using Eq. 1 with coefficients given in Table 4, **Background Data Set**[1]. (a) Experimental data from this study. Error bars at 1σ. (b) Experimental data from this (filled symbols) and previous (open symbols) studies [7].

The trend in Fig. 1a can be fit to an equation of the form:

$$\log\left[\mathrm{d}\frac{V_{melt}}{V_{sp}} - 1\right] = b\log_{fO_2} + c \qquad (1)$$

which was originally developed to describe Cr^{2+}–Cr^{3+} equilibria between spinel and basaltic melt [24] assuming that the abundance of Cr^{3+} is much greater than Cr^{2+} in spinel, which has since been demonstrated [25]. Eq. 1 has been used to describe V equilibria [7] but the assumption of only V^{3+} in spinel might appear invalid, as both V^{3+} and V^{4+}

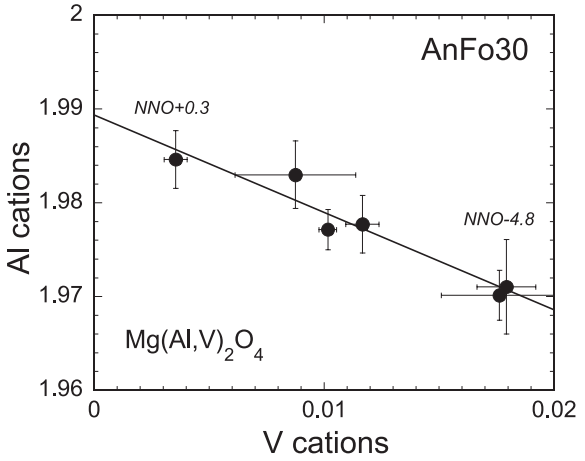

Fig. 2. Correlation of V and Al cations in spinel from AnFo30 composition. Error bars at 1σ. The trend of V with Al does not extrapolate to the 2.0 cations expected from spinel stoichiometry due to the small amount of Si in the spinels (Table 2, **Background Data Set**[1]).

spinels are well known [26]. The regular negative correlation between Al and V cations in spinels in the AnFo30 experiments, however, suggests that only V^{3+} substitutes for Al^{3+} in the octahedral site of spinel (Fig. 2) and that $D_V^{crystal/liq}$ for spinel and other mantle phases is governed by the availability of V^{3+} in the coexisting liquid. The increase in V^{3+} in spinel with decreasing fO_2 can further imply that if V^{2+} or V^{4+} exist in multicomponent melts they do not substitute into the spinel structure, and do not influence the value of $D_V^{sp/liq}$, at least over the range in fO_2 investigated.

In Eq. 1, the value of b is germane to the valence state of V in the melt phase and governing the partition. For example, if V^{3+} and V^{4+} are the prevailing valence states in the melt then the following equilibrium:

$$VO_{1.5} + 0.25O_2 \Leftrightarrow VO_2 \quad (2)$$

may be operative for which:

$$K = aVO_2/(aVO_{1.5}fO_2{}^{0.25}) \quad (3)$$

where K is the equilibrium constant and a is activity. Eq. 3 implies $D_V^{sp/liq}$ should scale to fO_2 by a factor b of 0.25. The experimental data shown in Fig. 1a were fit by multiple, non-linear regression to Eq. 2 assuming b is a constant of 0.25 (i.e. Eq. 2). The resultant fit provides a fair description of the data but if the b parameter is instead allowed to vary, the regressed values of b are invariably greater than 0.25 and a statistically better fit is achieved (Table 4, **Background Data Set**[1]). Values for b greater than 0.25 are suggestive of a valence change for V in the melt phase that is greater than 1.0, such as:

$$VO_{1.5} + 0.5O_2 \Leftrightarrow VO_{2.5} \quad (4)$$

for which b would equal 0.5. That the regressed values of b for the *auk* and *adk* komatiites (and other compositions described below) are intermediate between 0.25 and 0.5 (Table 4, **Background Data Set**[1]) suggest that equilibria between V^{3+}, V^{4+} and V^{5+} (i.e. both Eqs. 2 and 4) are operative in melts and control the partitioning of V over the fO_2 range of the experiments, contrary to the inference of only two valence states (V^{3+}, V^{4+}) proposed previously [7,13].

The change of $D_V^{sp/liq}$ with fO_2 in other mafic and ultramafic compositions are compared in Fig. 1b. All bulk compositions show similar trends that can be adequately fit by Eq. 1 but with different fit coefficients (d, b, c) for each composition (Table 4, **Background Data Set**[1]). There is a positive correlation between $D_V^{sp/liq}$ and Cr/Al ratio in spinel at constant fO_2 (Fig. 1b) which may result from a crystal chemical effect if the excess free energies of mixing of V–Cr spinels are lower than those of V–Al spinels. There are no thermochemical data on vanadiniferous spinel solid solutions but excess free energies of mixing of 3.2 and 12.9 kJ mol^{-1} are estimated for V–Cr and V–Al spinels, respectively, using a cation size mismatch approach [27] suggesting that this may indeed be the cause for correlations of $D_V^{sp/liq}$ with Cr/Al in spinel. Alternatively, an electronic exchange on the octahedral site ($Fe^{3+} + V^{3+} \Leftrightarrow Fe^{2+} + V^{4+}$) may be responsible for the correlations [27]. Both mechanisms are testable in experiments in simpler systems than examined in this study.

4.2. Garnet- and pyroxene-liquid

The results for $D_V^{gt/liq}$ in three experiments on

the KLB1 solidus are plotted for comparison with similar experimental data for garnet in komatiite melt, and for clinopyroxene (Fig. 3a). The levels of V in garnets measured by EMP in the current study are above 3σ of the background but the data are not particularly precise, whereas analyses of coexisting liquids for V by LA-ICP-MS are very accurate and precise. The $D_V^{gt/liq}$ values can thus be regarded as upper limits. Because fO_2 cannot be explicitly controlled in these high pressure experiments (only measured) there is not a large spread of data relative to the NNO buffer as is achievable in the 100 kPa experiments. Nonetheless, it is clear in all cases that V is mildly incompatible in garnet at conditions of ~NNO-3, and that $D_V^{gt/liq}$ is far less than that of clinopyroxene as suggested previously [12]. If the trend of $D_V^{gt/liq}$ follows that of other silicates, V will be even less compatible in garnet at higher fO_2.

The levels of V in 'pigeonitic' pyroxene on the peridotite solidus above 4.5 GPa are below detection limits of EMP, even using long counting times (Table 2, **Background Data Set**[1]). Estimates for $D_V^{pig/liq}$ for these experiments are also only upper limits. Only in experiment #361 (Table 3, **Background Data Set**[1]) were the pyroxene grains large enough to be analyzed by LA–ICP–MS to provide an accurate estimate of $D_V^{pig/liq}$. All data show that $D_V^{pig/liq}$ values along the mantle solidus are very similar to $D_V^{opx/liq}$ measured at 100 kPa (Fig. 3b).

5. Partial melting model

Experimental data for the fO_2 dependence of $D_V^{crystal/liq}$ for olivine, orthopyroxene and clinopyroxene [7,11–13] can be combined with new estimates for $D_V^{sp/liq}$, $D_V^{gt/liq}$, and $D_V^{pig/liq}$ to calculate the V abundance in mantle lithosphere with

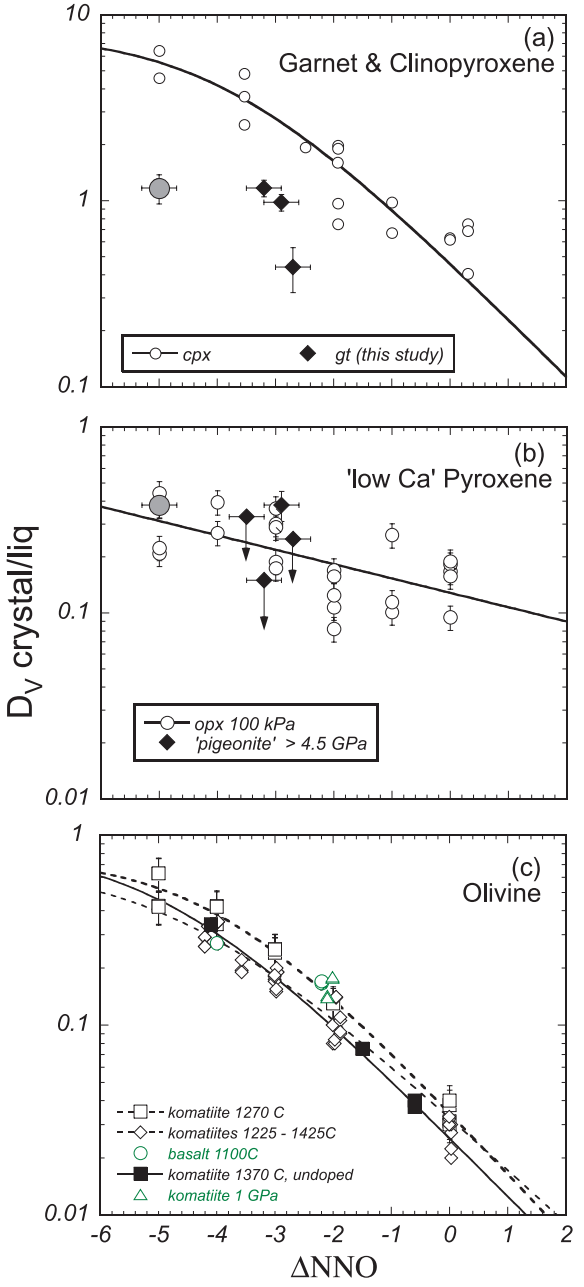

Fig. 3. Covariation of $D_V^{crystal/liq}$ with fO_2 for experiments in this study compared with published data. All trends are fitted to Eq. 1 with a variable b parameter except for low Ca pyroxene (Table 4, **Background Data Set**[1]). All error bars at 1σ. (a) Covariation of $D_V^{gt/liq}$ with fO_2 for experiments in this study compared with experimental data for $D_V^{cpx/liq}$ [12] and $D_V^{gt/liq}$ from (filled circle) [7]. (b) Covariation of $D_V^{pig/liq}$ with fO_2 for experiments in this study (solid diamonds) compared with experimental data for $D_V^{opx/liq}$ (open circles) and $D_V^{pig/liq}$ (filled circle) [7]. Note that $D_V^{pig/liq}$ values for three experiments are maxima (arrows). (c) Summary of the covariation of $D_V^{ol/liq}$ with fO_2 for experiments on various mafic and ultramafic compositions [7,11,13]. Error bars omitted here for clarity.

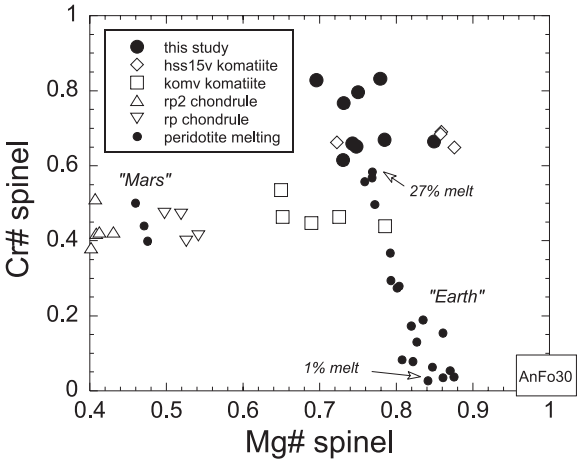

Fig. 4. Plot showing the Cr/Cr+Al (Cr#) versus Mg/Mg+Fe (Mg#) for spinels from experiments in which $D_V^{sp/liq}$ is measured (this study and) [7] compared to spinel compositions in the melting interval of terrestrial [28,29] and Martian mantle compositions [60] from ~1 to 30% partial melting. The AnFo30 spinels are not unlike near solidus spinels whereas the *auk* and *adk* spinels are similar to spinels in equilibrium with higher degree partial melts.

changing fO_2 during partial melting. In light of the new experimental results for spinel, previous experimental data for clinopyroxene, orthopyroxene and olivine were re-fit according to Eq. 1 with a variable *b* parameter that considers V^{3+}, V^{4+} and V^{5+} in melts (Fig. 3). At pressures above 2.8 GPa, $D_V^{gt/liq}$ was assumed a value of 1.0, and near-solidus 'pigeonitic' pyroxene is assumed to have a $D_V^{crystal/liq}$ of orthopyroxene (Fig. 3). The weighted $D_V^{residue/liq}$ at a given P, melt fraction and fO_2 was calculated by combining the stoichiometry of melting reactions along the peridotite solidus determined in experiments at 1.0, 1.5, 3.0 and 7 GPa [28–30] with experimentally measured $D_V^{crystal/liq}$ for phases stable on the solidus (Figs. 1 and 3). The value of $D_V^{sp/liq}$ was estimated to lie between the lower limit of the low Cr/Al AnFo30 data, which are not unlike near solidus aluminous spinels, to the higher Cr/Al *auk* and *adk* spinels similar to those stable well into the melting interval (Fig. 4).

The calculated V abundances in mantle residues as a function of fO_2 are compared with another element that measures melt depletion in the residue. Al is chosen as a depletion index because it is immobile during serpentinization, marine weathering and metamorphic processes that ensue during the exhumation of mantle peridotites [31] permitting samples from many different settings in all states of preservation to be compared with each other and with the partial melting model calculations. In addition, the behavior of Al during partial melting is coherent with that of V except that the latter may vary with fO_2. This geochemical coherency arises because V and Al show preference for the same mantle minerals, or the same lattice sites in a given mineral. The change in Al_2O_3 in the mantle residue with degree of melting at different pressures was modelled by treating Al as a mildly incompatible element. Chemical data for melts and residues in isobaric peridotite melting experiments were fit by linear regression and show changes in bulk $D_{Al_2O_3}^{residue/liq}$ with melt fraction at a given pressure (Table 5, **Background Data Set**[1], Fig. 5) that are consistent with the trends deduced from phase equilibria in simple systems [32].

The parameterized $D_{Al_2O_3}^{residue/liq}$ values are combined with weighted $D_V^{residue/liq}$ in the equation for non-modal, fractional melting [33] to calculate V and Al_2O_3 in the residue at a given melt fraction, fO_2 and pressure. The starting composition used in the calculations was primitive upper mantle (PUM) with 82 ppm V and 4.45 wt% Al_2O_3

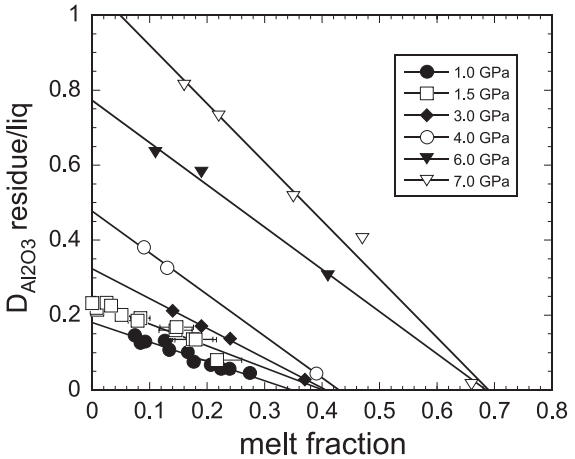

Fig. 5. Covariation of $D_{Al_2O_3}^{residue/liq}$ versus melt fraction at different pressures fitted by linear regression (Table 5, **Background Data Set**[1]). $D_{Al_2O_3}^{residue/liq}$ is calculated from mass balance of chemical data from peridotite melting experiments [28–30].

[34]. The essential equations for $D_V^{crystal/liq}$ of near-solidus minerals and for $D_{Al_2O_3}^{residue/liq}$ are given in Tables 4 and 5, **Background Data Set**[1].

Petrological studies of mantle melts and residues in the ocean basins show that melting in the mantle to form lithosphere is a polybaric, near-fractional process [33,35]. The model developed above is a combination of isobaric, equilibrium melting reactions with equations for fractional melting. It is empirical and clearly not a universal description of melting that can be extrapolated to a wide variety of scenarios in nature, but was necessarily simplistic because the current state of knowledge of peridotite phase relations and melting reactions determined by experiment does not afford a better description of the melting process to form a mantle residue. As emphasized by Walter [36] melting reactions on the solidus can only be derived from isobaric experiments, and such reactions will only be an approximation to the diverse set of changing reactions that must occur during polybaric, fractional melting in a real, multi-component mantle. The results of the polybaric, fractional melting process in nature should fall within the extremes of the isobaric, fractional cases considered in the models. This assumption seems to be a close approximation for the generation of many mantle-derived magmas [35] and is tested below where the model is applied to abyssal peridotite residues for which the melting conditions (P, fO_2, degree of depletion) and petrogenetic history are reasonably well understood [33,35,37].

6. Abyssal peridotites

The covariation of V with Al_2O_3 in abyssal peridotites[2] can be compared with calculated residue trends at 1.5 GPa assuming a constant $D_V^{sp/liq}$ (Fig. 6a) or two extreme values of $D_V^{sp/liq}$ for high- and low-Cr/Al spinels (Fig. 6b). The abyssal peridotite array is produced by 25–30% partial melting in both models, higher than that estimated for most abyssal samples [33,35,37] but this is mainly an effect of the Al_2O_3 assumed in the starting composition (PUM). If a more depleted source (e.g. 3.5 wt% Al_2O_3) is used in the calculations, the trend is the same with only 5–25% melting required to match the abyssal peridotite array, more consistent with petrologic data for natural samples. Because of the pressure dependence of melt reaction stoichiometry and the value of $D_{Al_2O_3}^{residue/liq}$ (Fig. 5), melting models at 1.0 GPa require a higher fO_2 to produce a given V–Al_2O_3 covariation (Fig. 6b). All spinel peridotite melting models, regardless of assumed pressure and $D_V^{sp/liq}$, fit the array of abyssal peridotite compositions quite well at fO_2s during melting that bracket those estimated thermobarometrically for mid-ocean ridge basalts and their complementary abyssal peridotite residues (NNO-1 to NNO-3 [6,9]).

Melting in the garnet stability field to produce MORB and abyssal peridotite residues is controversial [17,33]. Garnet peridotite melting at 7 GPa does not fit the trend of abyssal peridotite residues at any reasonable fO_2 (Fig. 6d) whereas results at 3 GPa are not unlike those at 1.5 GPa, and produce a reasonable approximation to the natural data at an fO_2 between NNO-2 and NNO-3 (Fig. 6c), consistent with thermobarometric estimates for natural samples.

The consistency of all of the calculated trends with the array of abyssal peridotite residues indicate that the empirical partial melting model developed using V and Al partitioning is a reasonable approximation to the natural case. Models at different pressures require different fO_2 to produce the same residue trend, but regardless of the model chosen, increased fO_2 during melting results in a clearly different V–Al covariation, with less V in the residue for a given level of melt extraction. This attribute of all the partial melting models can now be used to examine trends for mantle residues of other ages and geological settings.

7. Off-craton peridotites

Off-craton peridotites are considered in this

[2] A geochemical database ($n > 1200$) of these and other samples discussed in this paper is available upon request.

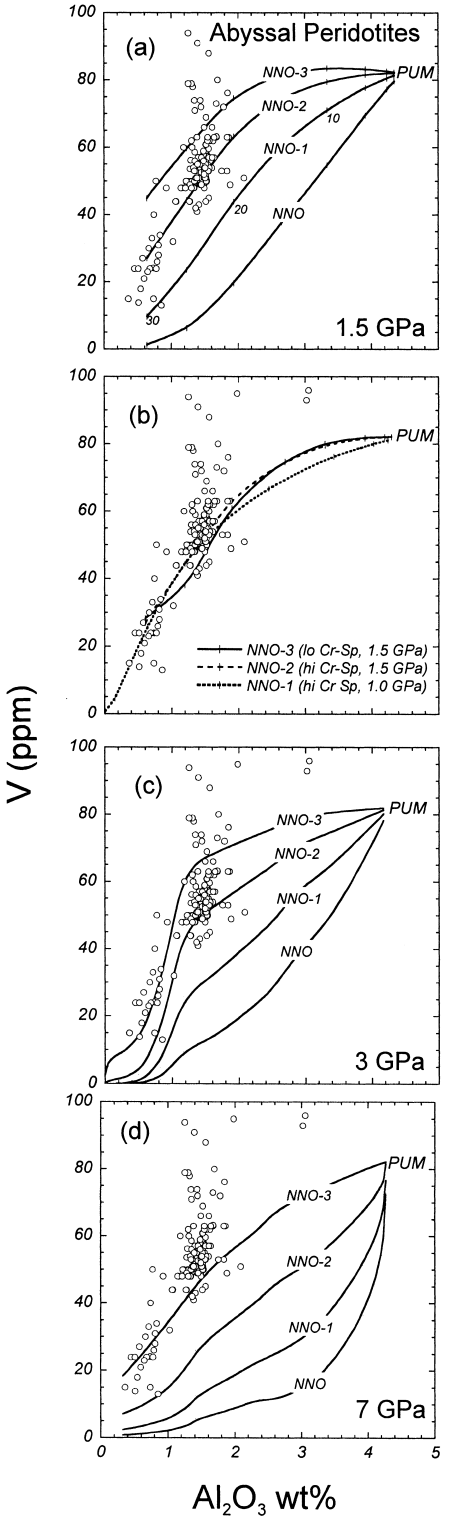

Fig. 6. Calculated covariation of V and Al_2O_3 in peridotite residues formed by different degrees of non-modal, fractional melting of PUM at different P and fO_2 conditions compared to compositions of natural abyssal peridotites. (a) Spinel peridotite melting models at 1.5 GPa showing effect of fO_2 assuming a $D_V^{sp/liq}$ for high-Cr/Al spinel. Tick marks and numbers along each trend show percentage melting. (b) Similar models showing effect of using different $D_V^{sp/liq}$ for high- versus low-Cr/Al spinel in the fractional melting equations and the effect of pressure. Use of a $D_V^{sp/liq}$ for low Cr/Al spinel (e.g. $D_V^{sp/liq}$ for AnFo30) decreases the fO_2 required to fit the residue trend. Decreased pressure requires an increase of $1\log fO_2$ unit to fit the trend. (c,d) Garnet peridotite melting models at 3.0 and 7 GPa.
←

study as peridotite xenoliths or massifs in Proterozoic to late Cenozoic orogenic belts, or as dredged samples in modern oceanic forearcs and subduction zones. Covariations of V and Al_2O_3 in these rocks are compared in Fig. 7 with partial melting trends for spinel peridotite at various fO_2 conditions. Most spinel peridotites from orogenic massifs are on average much less depleted than abyssal peridotite, ranging in composition from estimates for PUM to depleted compositions not unlike abyssal peridotites (Fig. 7a). Few orogenic spinel peridotites are colinear with the abyssal array, and most are shifted to the right of this array on the diagram, containing lower V for a given degree of depletion. The trend of orogenic peridotites is fairly coherent and generally one of melt depletion at $\sim 1\log fO_2$ unit greater than for abyssal peridotites.

Peridotites dredged from oceanic forearcs are depleted with less than ~ 1.5 wt% Al_2O_3, and plot along the abyssal array (Fig. 7a) whereas samples from active subduction zones such as in western Mexico are much less depleted. The Mexican samples plot along an array suggesting conditions of melting at one or two orders of magnitude higher fO_2 than beneath mid-ocean ridges, similar to the fO_2 recorded by mafic lavas from this region [6].

Off-craton spinel peridotite xenoliths are also on average far less depleted than abyssal peridotites, and like orogenic spinel peridotites, are shifted to the right of abyssal samples. When compared to orogenic peridotites, however, the xenolith suites show a pronounced dispersion to

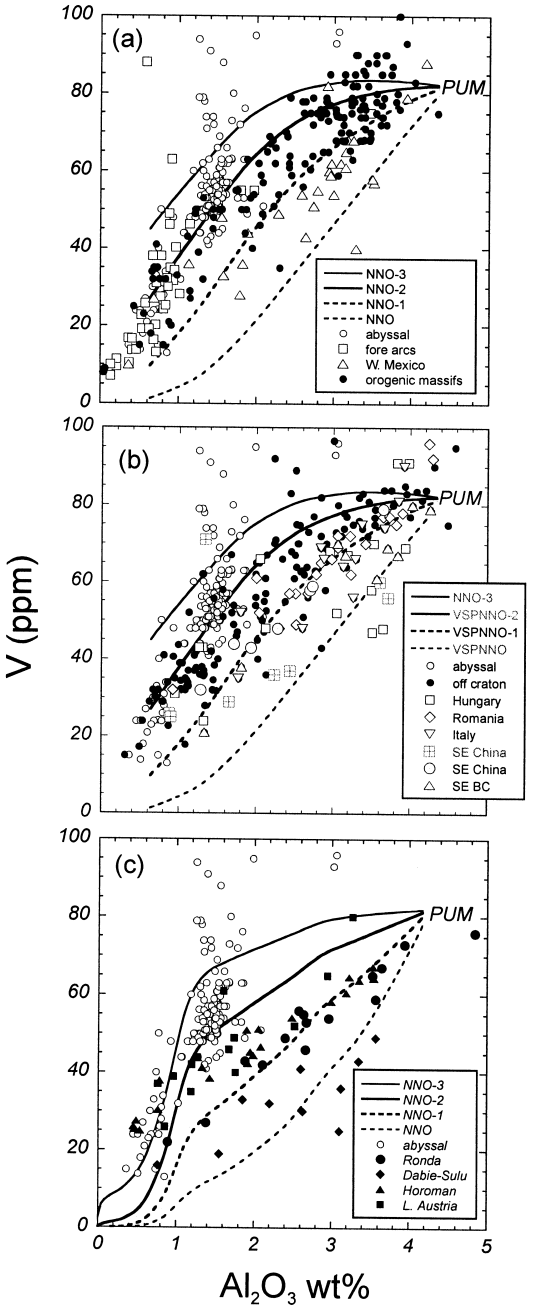

Fig. 7. Calculated residue trends at 1.5 GPa for a fO_2 conditions compared to samples of (a) spinel-bearing orogenic peridotite massifs, oceanic fore-arcs and subduction zone xenoliths and (b) off-craton spinel peridotite xenoliths. In (c) garnet-bearing orogenic peridotite massifs are compared with calculated residue trends at 3.0 GPa. The abyssal peridotite array from Fig. 6 is shown for reference.

lower V for a given degree of depletion (Al) (Fig. 7b). A significant population of off-craton xenoliths are colinear with the trend of less-depleted mantle from active subduction zones and are derived from tectonic environments that experienced variations in fO_2 during melting that are much larger than observed for orogenic massifs. Most of the xenolith suites shifted to the right of the orogenic array are from either young, active extensional terranes (S.E. China, Romania, Hungary) or areas that have experienced late Cenozoic subduction (southern British Columbia, Italy). The xenoliths are consistent with a range of fO_2 during depletion of over three orders of magnitude ($\sim$NNO to NNO-3).

Orogenic garnet peridotites from four massifs are compared with melting models for both spinel and garnet peridotite in Fig. 7c. The origin of these peridotites as either residues in the garnet- or spinel-facies is debated. Many of these bodies show an extremely complex tectonic and metamorphic history, and both the Ronda and Dabie-Sulu show petrological evidence for being exhumed from depths in excess of 150 km [38,39]. Intriguingly, all orogenic garnet peridotites are some of the most impoverished in V of the entire off-craton dataset. This distribution immediately raises the suspicion as to whether samples plotting to the right of the abyssal array in Fig. 7 truly reflect higher fO_2 during melting (and thus more incompatible behavior of V) or are simply related to the presence of garnet at the solidus at higher pressures. Recall from Fig. 6, however, that melting at 1.5 or and 3.0 GPa (i.e. spinel- versus garnet-facies) produces a similar array on this diagram, because garnet is consumed near the solidus at 3.0 GPa [30]. Therefore, even for garnet peridotite melting at 3.0 GPa, melting at higher fO_2 is still required to explain V and Al in garnet peridotite residues that plot far to the right of the abyssal array (Fig. 7c).

Both the Ronda and Horoman datasets are consistent with melt extraction at higher fO_2 than the abyssal peridotites. Indeed, both of these massifs have a V–Al_2O_3 distribution that is not unlike that of xenoliths from active subduction zones shown in Fig. 7a. Of particular geodynamic significance are the data for orogenic garnet peri-

dotites from the Dabie-Sulu terrane in east-central China. These particular peridotites show the lowest levels of V for a given degree of depletion and comparison of their trend to either spinel or garnet peridotite melting models show that the Dabie-Sulu rocks were likely produced at very high fO_2 ($\sim$NNO). An alternative interpretation is that they were produced at much higher pressures (7.0 GPa) at an fO_2 similar to that recorded by abyssal peridotites. The high fO_2 model, however, is more consistent with the numerous petrological and geological observations on peridotites from this terrane, which suggest they formed in the hanging- or footwall of a subduction zone, before being subducted to depths of the diamond stability field and later exhumed [39].

8. Cratonic peridotites

Cratonic peridotites are xenoliths with low temperatures of equilibration (<1200°C) and coarse textures, hosted in kimberlites from Archean cratons [40]. The Re–Os isotopic systematics in many cratonic peridotites show that they formed as residues in the Archean, and were isolated in the mantle 'roots' of cratons since that time [41]. As a separate type of lithospheric mantle, these rocks have a special place in discussions of the tectonic environment for the formation of deep mantle roots beneath Archean cratons.

A large proportion of cratonic peridotites contain significantly lower FeO than off-craton peridotites. The higher levels of depletion in cratonic lithosphere suggest that lithosphere-forming processes in the Archean occurred under greater degrees and/or higher pressures of melt extraction when compared to Phanerozoic examples [40]. Whether cratonic peridotites formed at high pressures in equilibrium with garnet, or at generally lower pressures by extraction of melts in the spinel stability field is debated [42–44] and can imply different tectonic settings for the formation of mantle lithosphere beneath Earth's first continents. Melt extraction at generally low pressures culminating in the spinel-facies is consistent with a large body of geochemical and petrological data [42,45,46] but is at odds with the low FeO of cratonic peridotites [43,44]. Information on the tectonic setting and redox state is essential in clarifying this issue and the V distributions in cratonic peridotites become useful in this debate.

Fig. 8 shows the covariation of V and Al_2O_3 in cratonic peridotites from five different cratons, with data from each craton separated according to peridotite-facies (garnet- or spinel-bearing). Overall, a significant population of cratonic peridotites have lower V abundances for a given degree of depletion when compared to abyssal peridotites, but there are subtle details for each craton (Fig. 8). If cratonic mantle lithosphere is considered a residue of primitive mantle, then spinel-bearing lithosphere beneath the Siberian and Kaapvaal cratons formed at higher fO_2 than lithosphere forming today beneath ocean ridges (Fig. 8a,b) and more like conditions similar to those in modern convergent margins. Interestingly, the Siberian and Kaapvaal datasets are also the only two suites that show consistently higher Si-enrichment and FeO depletion when compared to other mantle rocks, characteristics which have been attributed to processes in a convergent margin [42].

The covariation of V and Al for cratonic peridotites from other cratons shows somewhat varied patterns. Almost all spinel peridotites investigated from Tanzania are extremely depleted and plot along the abyssal array (Fig. 8d). Few spinel peridotites but almost all garnet peridotites from this craton are shifted to the right of the abyssal array, suggesting that the deeper parts of the Tanzanian lithosphere formed or was re-fertilized at a higher fO_2. This may have been related to re-activation of lower parts of the Tanzanian craton by propogation of the east African rift, as suggested by Re–Os isotopic systematics in xenoliths from this region [47].

The opposite trend is exhibited for peridotites from the Jericho kimberlite in the northern Slave craton, where the deeper garnet-bearing samples of the mantle lithosphere plot exclusively along the abyssal array, but many spinel peridotites from shallower levels record higher fO_2 during melting (Fig. 8c). The deeper garnet peridotites from beneath the northern Slave province might have formed as oceanic mantle lithosphere not

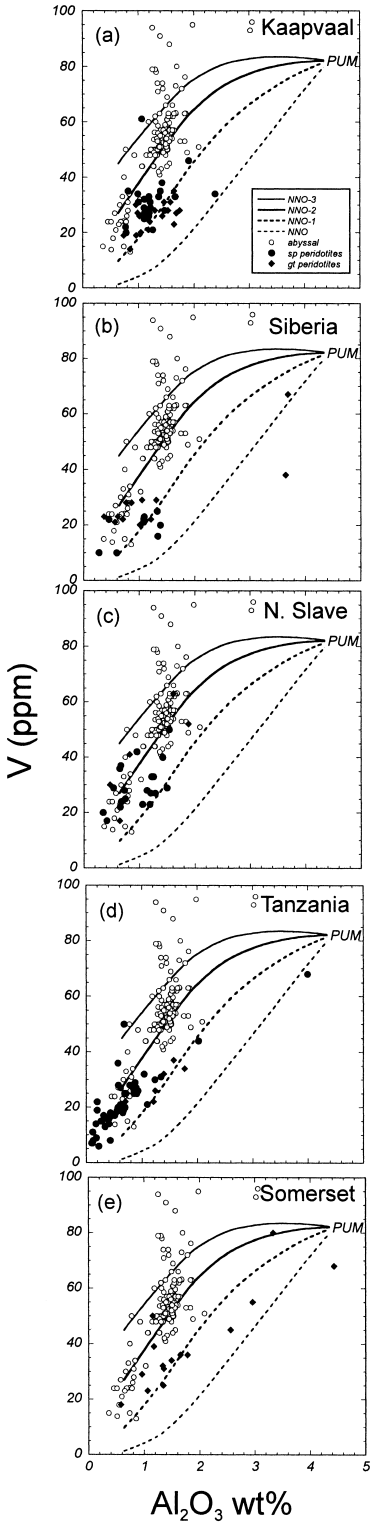

Fig. 8. Calculated residue trends at 1.5 GPa for a range of fO_2 conditions compared to compositions of both spinel- and garnet-bearing cratonic peridotites from (a) Kaapvaal, southern Africa, (b) Siberia, (c) northern Slave, Canada, (d) Tanzania, (e) Somerset Island, Canada. The abyssal peridotite array from Fig. 6 is shown for reference.
←

unlike that of abyssal peridotites, that has underthrust spinel-facies mantle formed in a more oxidized convergent margin setting. Convincing seismological and magnetotelluric evidence for low angle subduction to explain such a stratification exists beneath the Slave craton [48,49]. The Slave craton also shows significant stratification in its level of depletion [50–52] which may correlate with the redox state and tectonic provenance of the lithosphere that has been imbricated to form the craton root.

Interpretation of the V–Al array of garnet-facies mantle from Archean cratons in terms of its redox state and tectonic environment during formation is equivocal using the partial melting models in this study. If the unique FeO depletion in all cratons is attributed to melting at pressures greater than 3.0 GPa, [43,44] then the fO_2 during formation of Archean garnet peridotites need not be very high. Garnet peridotites from all Archean cratons plot along depletion trends at 7.0 GPa and fO_2 similar to those observed beneath modern mid-ocean ridges or hotspots (NNO-3 to NNO-2) (Fig. 9). Arguments to explain the high Cr/Al in garnets from these samples, however, implicate original melt depletion in the spinel-facies with subduction or underthrusting of lithosphere to conditions of garnet stability [45,46]. Such an interpretation would suggest that melting models at pressures at or below 3.0 GPa would apply to all peridotites from cratons, in which case the vast majority of the garnet-bearing samples would have formed at quite high fO_2 (Fig. 8).

The possibility that mantle lithosphere formed in the Archean under the oxidizing conditions of a convergent margin may lead to clues as to the origin of the unique and enigmatic FeO depletion in many cratonic peridotites. As noted above, spinel peridotite melting models can explain many attributes of these rocks, but fail to explain their low FeO. What has not been considered in

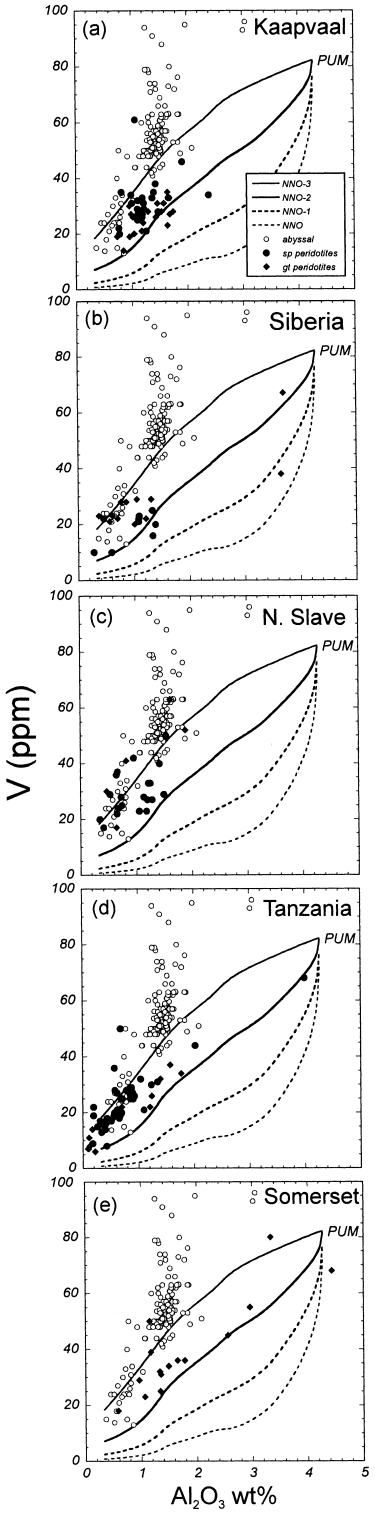

Fig. 9. Calculated residue trends at 7.0 GPa for a range of fO_2 conditions compared to compositions of both spinel- and garnet-bearing cratonic peridotites from (a) Kaapvaal, southern Africa, (b) Siberia, (c) northern Slave, Canada, (d) Tanzania, (e) Somerset Island, Canada. The abyssal peridotite array from Fig. 6 is shown for reference.
←

this discussion is the possibility that Archean mantle lithosphere formed by melting under more oxidized conditions than sub-oceanic lithosphere of younger age. The evidence above clearly shows this is a tenable scenario. Melting at higher fO_2 causes more Fe (as mildly incompatible Fe^{3+}) to enter the melt phase, leaving the residue with a greater Mg# for a given degree of melting than at lower fO_2. This hypothesis is testable given the requisite experimental data for peridotite melting under conditions of varying fO_2. Unfortunately, a mantle at 'FMQ' has become almost axiomatic in the petrological literature, and has confined experimental studies on mantle melting to restricted and generally reducing conditions, despite evidence that the fO_2 of mantle source regions may vary almost nine orders of magnitude [6]. This problem is partly attributable to technical limitations. For example, most experimental studies devoted to mantle melting are performed in graphite capsules, generating almost exclusively very low fO_2 conditions [53]. Analysis of mantle melts and residues may be biased by the experimental results of what are reduced fO_2 conditions when compared with most mantle samples. Although experimentally challenging, peridotite melting studies under more oxidizing conditions above 'FMQ' in the future can address the full implications of this variable for the origin of Archean and younger lithosphere.

9. Mantle redox, life and atmospheric evolution

The observations for Archean mantle residues, and complimentary work on Archean magmas [7,8,11] argue strongly that the conditions of mantle melting to form lithosphere in the Archean were just as oxidized as those of the more recent geologic past in various tectonic environments. These data might appear at odds with the very

reduced fO_2 recorded by sulfides included in diamonds [3,54] but the latter samples are not likely to be representative of the mantle as a whole. Many other inclusions in diamonds (native Fe, SiC) [55] attest to very extreme fO_2 conditions achieved in regions of the mantle which are not relevant to the formation of magmas or lithosphere.

The Earth's oldest microfossils occur in rocks 3.5 Ga old, and biomarkers are suggestive of even earlier forms of life [56]. Early Archean mantle redox is thus a period critical to discussions of the origin of life. Abiotic synthesis of molecules and hydrocarbons that can lead to life in early Archean mantle-derived volcanic gases requires they contain significant H_2 and CO, [57] but such reduced components are not supported by results of this and many other studies, which imply a scenario of Archean mantle redox not unlike that of today. Life may have found its origins in other environments or by other mechanisms.

Furthermore, the results above for Archean mantle lithosphere suggest that the mantle was oxidized early (by $\sim$3.5 Ga), so gradual oxidation of the solid Earth system by volcanic degassing of reduced species and ensuing H_2 escape [3] cannot have occurred. Gradual oxidation of the mantle by H_2O recycling during subduction is also implausible on petrological grounds [58]. It has been emphasized [3] that if the mantle did not become oxidized in the Archean then the atmosphere must itself have already been oxidized at this time. This scenario would be at odds with many interpretations of the geological evidence for atmospheric evolution. An answer to this conundrum is beyond the scope of this paper. What is clear, however, is that future models for prebiotic synthesis and the evolution of O_2 in the atmosphere must consider a more oxidized state of the Archean mantle.

Acknowledgements

This research was supported by NSERC of Canada and a Mercator Professorship from the German Science Foundation held at Ludwig-Maximilians Universität München. D.B. Dingwell is thanked for his hospitality, C.T. Lee for sharing some of his peridotite database, L. Shi and M. Raudsepp for assistance with EMP analyses, and J. Fan for assistance with LA-ICP-MS analyses. Finally, thanks to M. Walter and anonymous for reviews. *[BW]*

References

[1] M. Menzies, C. Dupuy, Orogenic massifs:protolith process and provenance, J. Petrol. Spec. Lherzolites Issue (1991) 1–16.
[2] E. Bonatti, P.J. Michael, Mantle peridotites from continental rifts to ocean basins to subduction zones, Earth Planet. Sci. Lett. 91 (1989) 297–311.
[3] J.F. Kasting, D.H. Eggler, S.P. Raeburn, Mantle redox evolution and the oxidation state of the Archean atmosphere, J. Geol. 101 (1993) 245–257.
[4] C. Lecuyer, Y. Ricard, Long-term fluxes and budget of ferric iron: implication for the redox states of the earth's mantle and atmosphere, Earth Planet. Sci. Lett. 165 (1999) 197–211.
[5] C. Ballhaus, Redox states of lithospheric and asthenospheric upper mantle, Contrib. Mineral. Petrol. 114 (1993) 331–348.
[6] I.S.E. Carmichael, The redox states of basic and silicic magmas: a reflection of their source regions?, Contrib. Mineral. Petrol. 106 (1991) 129–141.
[7] D. Canil, Vanadium partitioning between orthopyroxene spinel and silicate melt and the redox states of mantle source regions for primary magmas, Geochim. Cosmochim. Acta 63 (1999) 557–572.
[8] J. Delano, Redox history of the Earth's interior since $\sim$3900 Ma: implications for prebiotic molecules, Origin Life Evol. Biol. (2001), in press.
[9] D.A. Ionov, B.J. Wood, The oxidation state of subcontinental mantle: oxygen thermobarometry of mantle xenoliths from central Asia, Contrib. Mineral. Petrol. 111 (1992) 179–193.
[10] D. Canil, H.S.C. O'Neill, D.G. Pearson, R.L. Rudnick, W.F. McDonough, D.A. Carswell, Ferric iron in peridotites and mantle oxidation states, Earth Planet. Sci. Lett. 123 (1994) 205–220.
[11] D. Canil, Vanadium partitioning and the oxidation state of Archean komatiite magmas, Nature 389 (1997) 842–845.
[12] D. Canil, Y. Fedortchouk, Clinopyroxene-liquid partitioning for vanadium and the oxygen fugacity during formation of cratonic and oceanic mantle lithosphere, J. Geophys. Res. 105 (2000) 26003–26016.
[13] D. Canil, Y. Fedortchouk, Olivine-liquid partitioning for vanadium and other trace elements with applications to modern and ancient picrites, Can. Mineral. 39 (2001) 319–330.

[14] D.J. Lindstrom, Experimental Study of the Partitioning of Transition Metals between Clinopyroxene and Coexisting Silicate Liquids, Ph.D. thesis, University of Oregon, OR, 1976.
[15] D. Van der Wal, R.L.M. Vissers, Structural petrology of the Ronda peridotite, SW Spain: deformation history, J. Petrol. 37 (1996) 23–43.
[16] F.A. Frey, C.J. Suen, H.W. Stockman, The Ronda high temperature peridotitegeochemistry and petrogenesis, Geochim. Cosmochim. Acta 49 (1985) 2469–2491.
[17] J.A.C. Robinson, B.J. Wood, The depth of the spinel to garnet transition at the peridotite solidus, Earth Planet. Sci. Lett. 164 (1998) 277–284.
[18] E.F. Osborn, D.B. Tait, The system diopside–forsterite–anorthite, Am. J. Sci. Bowen Volume (1952) 413–433.
[19] I. Horn, S.F. Foley, S.E. Jackson, G.A. Jenner, Experimentally determined partitioning of high field strength and selected transition elements between spinel and basaltic melt, Chem. Geol. 117 (1994) 193–218.
[20] C. Bertka, J.R. Holloway, Pigeonite at solidus temperatures: implications for partial melting, J. Geophys. Res. 98 (1993) 19755–19766.
[21] D. Canil, Orthopyroxene stability along the peridotite solidus and the origin of cratonic lithosphere beneath southern Africa, Earth Planet. Sci. Lett. 111 (1992) 83–95.
[22] Z. Chen, D. Canil, H.P. Longerich, Automated in situ trace element analysis of silicate materials by laser ablation inductively coupled plasma mass spectrometry, Fresenius J. Anal. Chem. 368 (2000) 73–78.
[23] D.C. Rubie, S. Karato, H. Yan, H.S. O'Neill, Low differential stress and controlled chemical environment in multianvil high-pressure experiments, Phys. Chem. Mineral 20 (1993) 315–322.
[24] P.L. Roeder, I. Reynolds, Crystallization of chromite and chromium solubility in basaltic melts, J. Petrol. 32 (1991) 909–934.
[25] J. Li, H.S.C. O'Neill, F. Seifert, Subsolidus phase relations in the system $MgO–SiO_2–Cr–O$ in equilibrium with metallic Cr, and their significance for the petrochemistry of chromium, J. Petrol. 36 (1995) 107–132.
[26] D.B. Rogers, R.J. Arnott, A. Wold, J.B. Goodenough, The preparation and properties of some vanadium spinels, J. Phys. Chem. Solids 24 (1963) 347–360.
[27] H.S.C. O'Neill, A. Navrotsky, Cation distributions and thermodynamic properties of binary spinel solid solutions, Am. Mineral. 69 (1984) 733–753.
[28] M.B. Baker, E.M. Stolper, Determining the composition of high-pressure mantle melts using diamond aggregates, Geochim. Cosmochim. Acta 58 (1994) 2811–2827.
[29] J.A.C. Robinson, B.J. Wood, J.D. Blundy, The beginning of melting of fertile and depleted peridotite at 1.5 GPa, Earth Planet. Sci. Lett. 155 (1998) 97–111.
[30] M.J. Walter, Melting of garnet peridotite and the origin of komatiite and depleted lithosphere, J. Petrol. 39 (1998) 29–60.
[31] J.E. Snow, H.J.B. Dick, Pervasive magnesium loss by marine weathering of peridotite, Geochim. Cosmochim. Acta 59 (1995) 4219–4235.
[32] C.H. Herzberg, Generation of plume magmas through time: an experimental perspective, Chem. Geol. 126 (1995) 1–16.
[33] K.T.M. Johnson, H.J.B. Dick, N. Shimizu, Melting in the oceanic upper mantle an ion microprobe study of diopsides in abyssal peridotites, J. Geophys. Res. 95 (1990) 2661–2678.
[34] W.F. McDonough, S.S. Sun, The composition of the earth, Chem. Geol. 120 (1995) 223–253.
[35] C.H. Langmiur, E.M. Klein, T. Plank, Petrological systematics of mid-ocean ridge basalts: constraints on melt generation beneath ocean ridges, in: J. Phipps Morgan, D.K. Blackman, J.M. Sinton (Eds.), Mantle Flow and Melt Generation at Mid-ocean Ridges, Monograph 71, American Geophysical Union, 1992, pp. 183–280.
[36] M.J. Walter, Comments on 'mantle melting and melt extraction processes beneath ocean ridges evidence from abyssal peridotites' by Yaoling Niu, J. Petrol. 40 (1999) 1187–1193.
[37] M.B. Baker, J.R. Beckett, The origin of abyssal peridotites: a reinterpretation of constraints based on primary bulk compositions, Earth Planet. Sci. Lett. 171 (1999) 49–61.
[38] G. Davies, P.H. Nixon, D.G. Pearson, M. Obata, Tectonic implications of graphitized diamonds from the Ronda peridotite massif, southern Spain, Geology 21 (1993) 471–474.
[39] R.Y. Zhang, J.G. Liou, J.S. Yang, T.-F. Yui, Petrochemical constraints for dual origin of garnet peridotites from the Dabie-Sulu UHP terrane, eastern-central China, J. Metam. Geol. 18 (2000) 149–166.
[40] F.R. Boyd, Compositional distinction between oceanic and cratonic lithosphere, Earth Planet. Sci. Lett. 96 (1989) 15–26.
[41] D.G. Pearson, The age of continental roots, Lithos 48 (1999) 171–194.
[42] P.B. Kelemen, S.R. Hart, S. Bernstein, Silica enrichment in the continental upper mantle via melt/rock reaction, Earth Planet. Sci. Lett. 164 (1998) 387–406.
[43] C. Herzberg, Phase equilibrium constraints on the formation of cratonic mantle, in: Y. Fei, C. Bertka, B.O. Mysen (Eds.), Mantle Petrology: Field Observations and High Pressure Experimentation, vol. 6, The Geochemical Society, Washington, DC, 1999, pp. 241–250.
[44] M.J. Walter, Melting residues of fertile peridotite and the origin of cratonic lithosphere, in: Y. Fei, C. Bertka, B.O. Mysen (Eds.), Mantle Petrology: Field Observations and High Pressure Experimentation, vol. 6, The Geochemical Society, Washington, DC, 1999, pp. 225–240.
[45] D. Canil, K. Wei, Constraints on the origin of mantle-derived low Ca garnets, Contrib. Mineral. Petrol. 109 (1992) 421–430.
[46] T. Stachel, K.S. Viljoen, G. Brey, J.W. Harris, Metasomatic processes in lherzolitic and harzburgitic domains of diamondiferous lithospheric mantle REE in garnets from

xenoliths and inclusions in diamonds, Earth Planet. Sci. Lett. 159 (1998) 1–12.
[47] J.T. Chesley, R.L. Rudnick, C.-T. Lee, Re–Os systematics of mantle xenoliths from the East African Rift age structure and history of the Tanzanian craton, Geochim. Cosmochim. Acta 63 (1999) 1203–1217.
[48] M.G. Bostock, Mantle stratigraphy and evolution of the Slave province, J. Geophys. Res. 103 (1998) 21183–21200.
[49] A.G. Jones, I.J. Ferguson, A.D. Chave, R.L. Evans, G.W. McNeice, Electric lithosphere of the Slave craton, Geology 29 (2001) 423–426.
[50] M. Kopylova, J.K. Russell, Chemical stratification of cratonic ithosphere: constraints from the northern Slave craton, Canada, Earth Planet. Sci. Lett. 181 (2000) 71–87.
[51] W.L. Griffin, B.J. Doyle, C.G. Ryan, N.J. Pearson, S. O'Reilly, R. Davies, K. Kivi, E. van Achterbergh, L. Natapov, Layered mantle lithosphere in the Lac de Gras area. Slave craton composition, structure and origin, J. Petrol. 40 (1999) 705–727.
[52] G.B. Carbno, D. Canil, Mantle structure beneath the southwest Slave craton, Canada: constraints from garnet geochemistry in the Drybones Bay kimberlite, J. Petrol. (2002), in press.
[53] J.R. Holloway, V. Pan, G. Gudmundsson, High pressure fluid-absent melting experiments in the presence of graphite: oxygen fugacity, ferric/ferrous ratio and dissolved CO_2, Eur. J. Mineral. 4 (1992) 105–114.
[54] D.H. Eggler, J.P. Lorand, Mantle sulfide geobarometry, Geochim. Cosmochim. Acta 57 (1993) 2213–2222.
[55] S.E. Haggerty, A diamond trilogy superplumes supercontinents and supernovae, Science 285 (2000) 851–860.
[56] J.J. Brocks, G.A. Logan, R. Buick, R.E. Summons, Archean molecular fossils and the early rise of eukaryotes, Science 285 (1999) 1033–1036.
[57] M. Zolotov, E.L. Shock, A thermodynamic assessment of the potential synthesis of condensed hydrocarbons during cooling and dilution of volcanic gases, J. Geophys. Res. 105 (2000) 539–559.
[58] B.R. Frost, C.H. Ballhaus, Comment on 'Constraints on the origin of the oxidation state of mantle overlying subduction zones: An example from Simcoe, Washington, USA' by A.D Brandon and D.S. Draper, Geochim. Cosmochim. Acta 62 (1998) 329–331.
[59] B.R. Frost, Introduction to oxygen fugacity and its petrologic significance, in: D.H. Lindsley (Ed.), Oxide Minerals: Petrologic and Magnetic Significance, Rev. Mineralogy 25, Mineral. Soc. Am., Washington, DC, 1991, pp. 1–10.
[60] C. Bertka, J.R. Holloway, Anhydrous partial melting of an iron-rich mantle I: subsolidus phase assemblages and partial melting phase relations at 10 to 30 kbar, Contrib. Mineral. Petrol. 115 (1994) 313–322.